21st Australasian Fluid Mechanics Conference
Adelaide, Australia
10-13 December 2018

Ultimate thermal turbulence and asymptotic ultimate turbulence induced by wall-roughness

Xiaojue Zhu, Ruben A. Verschoof, Dennis Bakhuis, Varghese Mathai, Sander G. Huisman, Richard J. A. M. Stevens, Roberto Verzicco, Chao Sun, Detlef Lohse

Physics of Fluids Group and Max Planck Center for Complex Fluid Dynamics, MESA+ Institute and J. M. Burgers Centre for Fluid Dynamics, University of Twente, P.O. Box 217, 7500AE Enschede, The Netherlands

Abstract

Turbulence is omnipresent in Nature and technology, governing the transport of heat, mass, and momentum on multiple scales. One of the paradigmatic turbulent flows is Rayleigh-Bénard convection, i.e., a flow heated from below and cooled from above. Here, the possible transition to the so-called ultimate regime, wherein both the bulk and the boundary layers are turbulent, has been an outstanding issue, since the seminal work by Kraichnan [Phys. Fluids 5, 1374 (1962)]. Yet, when this transition takes place and how the local flow induces it is not fully understood. By performing two-dimensional simulations of Rayleigh-Bénard turbulence covering six decades in Rayleigh number Ra up to 10^{14} for Prandtl number $\mathrm{Pr} = 1$, for the first time in numerical simulations we find the transition to the ultimate regime, namely at $\mathrm{Ra}^* = 10^{13}$. We reveal how the emission of thermal plumes enhances the global heat transport, leading to a steeper increase of the Nusselt number than the classical Malkus scaling $\mathrm{Nu} \sim \mathrm{Ra}^{1/3}$ [Proc. R. Soc. London A 225, 196 (1954)]. Beyond the transition, the mean velocity profiles are logarithmic throughout, indicating turbulent boundary layers. In contrast, the temperature profiles are only locally logarithmic, namely within the regions where plumes are emitted, and where the local Nusselt number has an effective scaling $\mathrm{Nu} \sim \mathrm{Ra}^{0.38}$, corresponding to the effective scaling in the ultimate regime.

For real-world applications of wall-bounded turbulence, the underlying surfaces are virtually always rough; yet characterizing and understanding the effects of wall roughness for turbulence remains an elusive challenge. By combining extensive experiments and numerical simulations, here, taking as 2nd example the paradigmatic Taylor-Couette system (the closed flow between two independently rotating coaxial cylinders), we uncover the mechanism that causes the considerable enhancement of the overall transport properties by wall roughness. If only one of the walls is rough, we reveal that the bulk velocity is slaved to the rough side, due to the much stronger coupling to that wall by the detaching flow structures. If both walls are rough, the viscosity dependence is thoroughly eliminated and we thus achieve what we call *asymptotic ultimate turbulence*, i.e. the upper limit of transport, in which the scalings laws can be extrapolated to arbitrarily large Reynolds numbers.

This Proceeding contribution summarizes and reproduces the main results of our recent references [56, 57].

Introduction

Rayleigh-Bénard (RB) flow, in which the fluid is heated from below and cooled from above, is a paradigmatic representation of thermal convection, with many features that are of interest in natural and engineering applications. Examples range from astrophysical and geophysical flows to industrial thermal flows [3, 26, 7]. When the temperature difference between the two plates (expressed in dimensionless form as the Rayleigh number Ra) is large enough, the system is expected to undergo a transition from the so-called "classical regime" of turbulence, where the boundary layers (BLs) are of laminar type[47, 55, 54, 8], to the so-called "ultimate regime", where the BLs are of turbulent type, as first predicted by Kraichnan [24] and later by others [43, 11, 12, 13, 14]. In the classical regime, the Nusselt number Nu (dimensionless heat transfer) is known to effectively scale as Ra^{β}, with the effective scaling exponent $\beta \leq 1/3$ [11, 12, 45, 27, 37]. Beyond the transition to the ultimate regime, the heat transport is expected to increase substantially, reflected in an effective scaling exponent $\beta > 1/3$ [24, 3, 13].

Hitherto, the evidence for the transition to the ultimate regime has only come from experimental measurements of Nu. In fact, the community is debating at what Ra the transition starts and even whether there is a transition at all. For example, in ref. [30] it was observed that β first increases above 1/3 around $\mathrm{Ra} \approx 10^{14}$ and then decreases back to 1/3 again for $\mathrm{Ra} \approx 10^{15}$. Subsequently, Urban *et al.* [48] also reported $\beta \approx 1/3$ for $\mathrm{Ra} = [10^{12}, 10^{15}]$. However, Chavanne *et al.* [5, 6] found that the effective scaling exponent β increases to 0.38 for $\mathrm{Ra} > 2 \times 10^{11}$. In the experiments mentioned above, low temperature Helium was used as the working fluid and Prandtl number Pr changes with increasing Ra. In contrast, using high pressure SF_6 which has roughly pressure independent Pr instead of Helium, a more conclusive realization of ultimate regime was achieved by He *et al.* [18, 17], who observed a similar exponent 0.38, but this exponent was found only to start at a much higher $\mathrm{Ra} \approx 10^{14}$ (the transition starts at $\mathrm{Ra} \approx 10^{13}$). This observation is compatible with the theoretical prediction [11, 12] for the onset the ultimate regime. It is also consistent with the theoretical prediction of Refs. [24, 13], according to which logarithmic temperature and velocity BLs are necessary to obtain an effective scaling exponent $\beta \approx 0.38$ for that Ra. The apparent discrepancies among various high Ra RB experiments have been attributed to many factors. The change of Pr, the non-Boussinesq effect, the use of constant temperature or constant heat flux condition, the finite conductivity of the plates, and the sidewall effect can all play different roles [3, 44].

Direct numerical simulations of 2D RB

Direct numerical simulations (DNS), which do not have these unavoidable artefacts as occurring in experiments, can ideally help to understand the transition to the ultimate regime, with the strict accordance to the intended theoretic RB formulations. Unfortunately, high Ra simulations in three dimensions (3D) are prohibitively expensive [41, 46]. The highest Rayleigh number achieved in 3D RB simulations is 2×10^{12} [44], which is one order of magnitude short of the expected transitional Ra. Two-dimensional (2D) RB simulations, though different from 3D ones in terms of integral quantities for small Pr [39, 51], still capture the many essential features of 3D RB [51]. Consequently, in recent years, 2D DNS has been widely used to test theories, not only for normal RB [20, 53], but also for RB in porous media [19]. Although also expensive at high Ra, now we have the chance to push forward to $\mathrm{Ra} = 10^{14}$ using 2D simulations. Another advantage of DNS as compared to experiment is that velocity and temperature profiles can be easily measured, to check whether they are logarithmic in the ultimate regime, as expected from theory. Specifically, for the temperature, only a few *local* experimental measurements were available in the near-sidewall regions of RB cells, which showed logarithmic profiles [1, 2]. Even worse, for velocity, there is almost no evidence for the existence of a logarithmic BL, due to the experimental challenges. For instance, in cylindrical cells with aspect ratio $\Gamma = O(1)$, the mean velocity profile cannot be easily quantified because of the absence of a stable mean roll structure [24]. In situations where stable rolls do exist (e.g. narrow rectangular cells), the highest Ra available are still far below the critical Ra at which logarithmic velocity BLs can manifest themselves [47, 8].

As numerical simulations provide us with every detail of the flow field which might be unavailable in experiments, they also enable us to reveal the links between the global heat transport and the local flow structures. A few attempts (both 2D and 3D) have been made in the classical regime, in which logarithmic temperature BLs were detected, by selectively sampling the regions where the plumes are ejected to the bulk [1, 49]. However, it is still unclear how these local logarithmic BLs contribute to the attainment of the global heat transport enhancement during the transition to the ultimate regime.

In ref. [56] we have observed a transition to the ultimate regime in 2D, namely at $\mathrm{Ra}^* = 10^{13}$, similar as in the 3D RB experiments of Ref. [18]. The DNS of [56] have provided evidence that the mean velocity profiles follow the log-law of the wall, in analogy to other paradigmatic turbulent flows, e.g. pipe, channel, and boundary flows [35, 28, 42]. In Fig. 1, we show Nu(Ra) compensated with $\mathrm{Ra}^{0.35}$, for the range Ra=$[10^8, 10^{14}]$. Up to Ra = 10^{11} (blue symbol), the effective scaling is essentially the same ($\beta \approx 0.29$) as has been already observed [23, 51, 50] in the classical regime where the BLs are laminar [55, 54]. This trend continues up to the transitional Rayleigh number $\mathrm{Ra}^* = 10^{13}$ (green symbol). Beyond this, we witness the start of the transition to the ultimate regime, with a notably larger effective scaling exponent $\beta \approx 0.35$, as evident from the plateau in the compensated plot.

We next focus on the mean velocity field at the transitional Ra. Remarkably, even after 500 dimensionless time units, the flow domain still shows a stable mean roll structure, i.e. the rolls are pinned with clearly demarcated plume ejecting and impacting regions. The mean temperature and velocity fields display horizontal symmetry, which enables us to average them over a single LSR instead of the whole domain (as the velocity averaged horizontally for the whole domain will be zero). Figure 2 shows the temporally and spatially averaged velocity profiles, performed on one single LSR. We plot the profiles in dimensionless wall units, in terms of u^+ and y^+, where $u^+ = \langle u \rangle_{x,t}/u_\tau$ and $y^+ = z u_\tau/\nu$. Here u_τ is the friction velocity $u_\tau = \sqrt{\nu \partial_z \langle u \rangle_{x,t}|_{z=0}}$ [36]. Similar to channel, pipe, and boundary layer flows, we can identify two distinct layers: a viscous sub-layer where $u^+ = y^+$, followed by a logarithmic region, where the velocity profile follows $u^+ = \frac{1}{\kappa_v} \ln y^+ + B_v$ [36]. The inverse slope gives $\kappa_v = 0.4$, which is remarkably close to the Kármán constant in various 3D canonical wall-bounded turbulent flows [28, 42]. However, the parameter B_v varies with Ra. With increasing Ra, the logarithmic range grows in spatial extent, until at $\mathrm{Ra}^* = 10^{13}$, it spans one decade in y^+.

We next explain how the global heat transport scaling can still undergo a transition to the ultimate regime, though only the local temperature profile is logarithmic, not the globally averaged one. We recall that by definition on the plate surface, Nu $= -\langle \partial_z \theta \rangle_A$. We compute the local Nu on the plate surface from ejecting (Nu_e) and impacting (Nu_i) regions separately. These are shown in Fig. 3, compensated by $\mathrm{Ra}^{1/3}$. Up to Ra^*, both Nu_i and Nu_e follow a similar trend, with their respective local scaling exponents β_i and $\beta_e < 1/3$. However, beyond Ra^*, Nu_i and Nu_e diverge. The ejecting regions show an increased heat transport, with $\beta_e = 0.38$, which is precisely the ultimate scal-

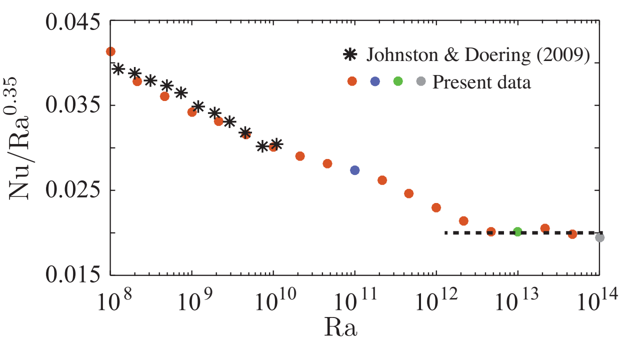

Figure 1: Nu(Ra) plot compensated by $\mathrm{Ra}^{0.35}$. A clear transition can be seen at Ra = 10^{13}, as evident from the plateau. The data agree well with the previous results in the low Ra regime [23]. The flow structures of the three colored data points (blue for Ra = 10^{11}, green for Ra = 10^{13}, grey for Ra = 10^{14}) are displayed in Fig. 2 of ref. [56].

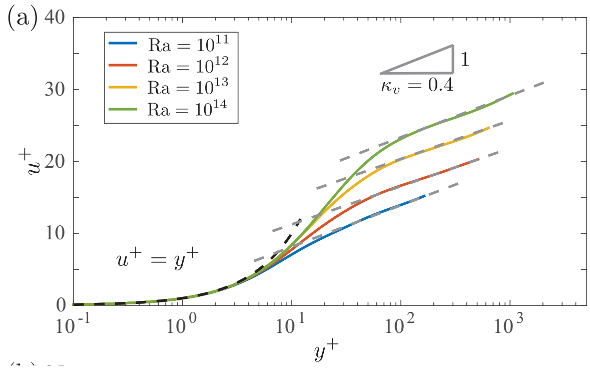

Figure 2: Mean velocity profiles in wall units (u^+ for velocity and y^+ for wall distance) at four Ra. The dashed lines show the viscous sublayer behavior and the log-layer behavior. A log-layer is seen for the velocity (with inverse slope $\kappa_v = 0.4$), but not for the temperature.

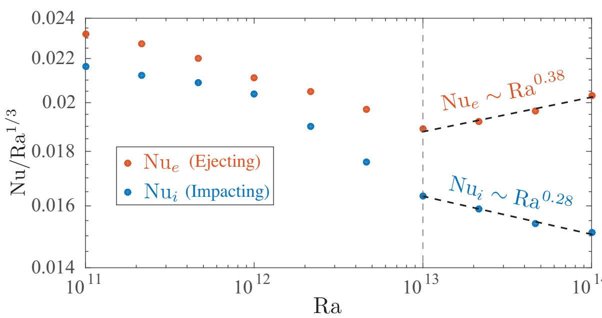

Figure 3: Local wall-heat-flux as a function of Ra, separately for the plume ejecting region (Nu_e) and the plume impacting region (Nu_i). At $\mathrm{Ra}^* = 10^{13}$, Nu_e starts to undergo a transition to the ultimate regime with an effective scaling exponent of 0.38, while Nu_i(Ra) has a much smaller effective scaling exponent of 0.28. The competition between the two parts finally determines the effective global scaling exponent.

ing exponent predicted for $\mathrm{Ra} \sim O(10^{14})$ with logarithmic BLs. In contrast, the impacting regions have a much lower scaling exponent $\beta_i = 0.28$. This means that the flow is partially in the ultimate regime and partially still in the classical regime.

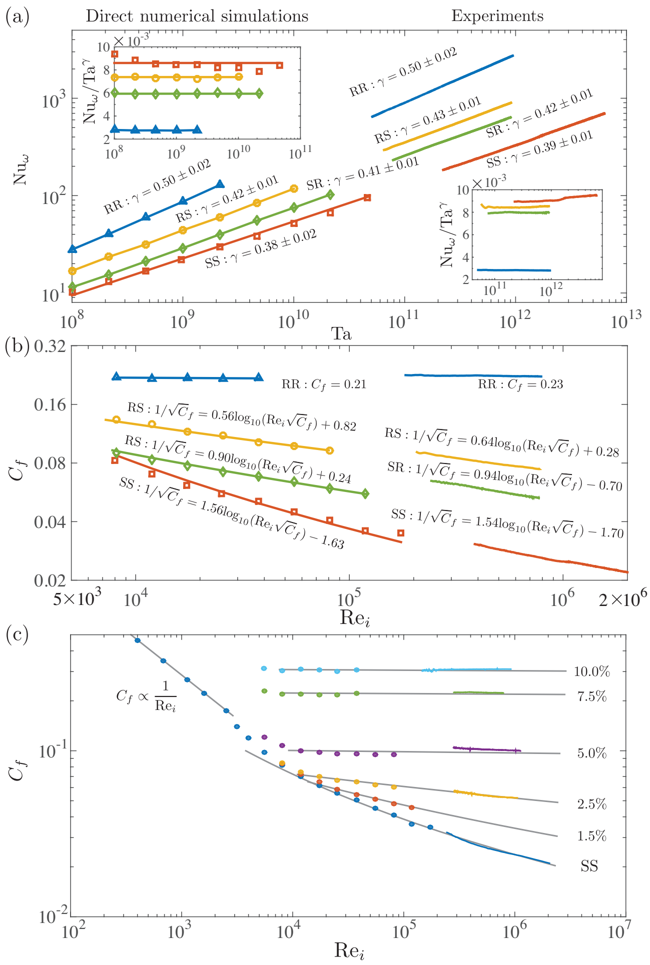

Figure 4: **Global torque and friction factor scalings in both DNS (symbols), and experiments (colored lines). a,** The dimensionless torque as a function of Taylor number Ta. Four cases are shown: (SS) both cylinders smooth; (SR) smooth inner, rough outer; (RS) rough inner, smooth outer; and (RR) both cylinders rough, with the exponent γ in the power law relation $\mathrm{Nu}_\omega \sim \mathrm{Ta}^\gamma$ shown for every case. The insets depict the compensated plots Nu/Ta^γ, showing the quality of the scaling. **b,** The friction factor c_f as a function of the inner cylinder Reynolds number Re_i. The lines show the best fits of the Prandtl friction law $1/\sqrt{c_f} = a\log_{10}(Re_i\sqrt{c_f}) + b$, with all prefactors shown in the figures. For **a** and **b**, 6 ribs were used and the roughness height is $h = 0.075d$. For the RR case, Re_i independent friction factors are revealed. **c,** The friction factor c_f for RR cases with 6 ribs of different heights, ranging from 1.5% to 10% of the gap width d.

Torque scaling in rough-wall Taylor-Couette flow

We address, both numerically and experimentally, the question of how roughness modifies the global scaling relations. For that, we choose the Taylor-Couette system [16], which is analogous to the RB system [9]. Ribs of varying height and distance represent the roughness. The results here are all taken from ref. [57]. First, we focus on the cases of 6 ribs with identical heights $h = 0.075d$, both numerically and experimentally. The global dimensionless torques, $Nu \sim Ta^\gamma$, for the four cases, with increasing Ta and fixed outer cylinder, are shown in Fig. 4a. Combining EXPs and DNSs, the range of Taylor number studied here extends over five decades. Similarly to what was shown in various recent studies [18, 52, 32, 33, 4, 16], for the SS case, an effective scaling of $Nu \sim Ta^{0.38\pm0.02}$ is observed in the DNS, corresponding to the ultimate regime with logarithmic corrections [24, 13]. A very similar scaling exponent $Nu \sim Ta^{0.39\pm0.01}$ is found in EXPs, demonstrating the excellent agreement between DNS and EXPs.

Dramatic enhancements of the torques are clearly observed with the introduction of wall roughness, resulting in the transition of Nu from $O(10^2)$ to $O(10^3)$. Specifically, when only a single cylinder is rough, the logarithmic corrections decrease and the scaling exponents marginally increase, implying that the scaling is dominated by the single smooth wall. For the RR case, the best power law fits give $Nu \sim Ta^{0.50\pm0.02}$, both for the numerical and experimental data, suggesting that the logarithmic corrections are thoroughly canceled. This state with the scaling exponent $1/2$ corresponds to the *asymptotic ultimate turbulence* predicted by Kraichnan [24]. The compensated plots of insets of Nu/Ta^γ show the robustness and the quality of the scalings.

When expressing the relation between the global transport properties and the driving force in terms of the Reynolds number dependence of the friction factor c_f, we obtain Fig. 4b. For the SS case, the fitting parameters a and b yield a von Kármán constant $\kappa = 0.44 \pm 0.01$, which is slightly larger than the standard value of 0.41 due to the curvature effect [21, 34, 15]. This agrees very well with the previous measurements on TC with smooth walls [25]. For the RR case, in both DNS and EXP, for large enough driving the friction factor c_f is found to be independent of Re_i, but dependent on roughness height, namely $c_f = 0.21$ in the DNS and $c_f = 0.23$ in the EXP for roughness height $h = 0.075d$, thus showing good agreement also for the rough cases. The results here are consistent with the asymptotic ultimate regime scaling $1/2$ for Nu and indicate that the Prandtl-von Kármán log-law of the wall [38, 36] with wall roughness can be independent of Re_i [31, 38, 36, 22, 10], which has been verified recently for Taylor-Couette flow [58]. For the RS and SR cases, one boundary is rough and the other is smooth such that the friction law lies in between RR and SS lines.

We further show the RR case with ribs of different heights, ranging from 1.5% to 10% of the gap width d in Fig. 4c, displaying its similarity with the Nikuradse [31] and Moody [29] diagrams for pipe flow. It can be seen that once $h \geqslant 0.05d$ and $\mathrm{Re}_i \geqslant 8.1 \times 10^3$ ($Ta \geqslant 10^8$), the asymptotic ultimate regime can always be achieved in both DNS and EXP.

Acknowledgements

The work is financially supported by the Dutch Foundation for Fundamental Research on Matter (FOM), the Netherlands Center for Multiscale Catalytic Energy Conversion (MCEC), the Dutch Technology Foundation (STW) and a VIDI grant (No. 13477), all sponsored by the Netherlands Organisation for Scientific Research (NWO). We thank the Dutch Supercomputing Consortium SurfSARA, the Italian supercomputer FERMI-CINECA through the PRACE Project No. 2015133124 and the ARCHER UK National Supercomputing Service through the DECI Project 13DECI0246 for the allocation of computing time.

References

[1] Ahlers, G., Bodenschatz, E., Funfschilling, D., Grossmann, S., He, X., Lohse, D., Stevens, R. J. A. M. and

Verzicco, R., Logarithmic temperature profiles in turbulent Rayleigh-Bénard convection, *Phys. Rev. Lett.*, **109**, 2012, 114501.

[2] Ahlers, G., Bodenschatz, E. and He, X., Logarithmic temperature profiles of turbulent Rayleigh-Bénard convection in the classical and ultimate state for a prandtl number of 0.8, *J. Fluid Mech.*, **758**, 2014, 436–467.

[3] Ahlers, G., Grossmann, S. and Lohse, D., Heat transfer and large scale dynamics in turbulent Rayleigh-Bénard convection, *Rev. Mod. Phys.*, **81**, 2009, 503.

[4] Brauckmann, H. J. and Eckhardt, B., Direct numerical simulations of local and global torque in Taylor-Couette flow up to Re = 30 000, *J. Fluid Mech.*, **718**, 2013, 398–427.

[5] Chavanne, X., Chilla, F., Castaing, B., Hebral, B., Chabaud, B. and Chaussy, J., Observation of the ultimate regime in Rayleigh-Bénard convection, *Phys. Rev. Lett.*, **79**, 1997, 3648–3651.

[6] Chavanne, X., Chilla, F., Chabaud, B., Castaing, B. and Hebral, B., Turbulent Rayleigh-Bénard convection in gaseous and liquid he, *Phys. Fluids*, **13**, 2001, 1300–1320.

[7] Chilla, F. and Schumacher, J., New perspectives in turbulent Rayleigh-Bénard convection, *Eur. Phys. J. E*, **35**, 2012, 58.

[8] du Puits, R. and Willert, C., The evolution of the boundary layer in turbulent rayleigh-bénard convection in air, *Phys. Fluids*, **28**, 2016, 044108.

[9] Eckhardt, B., Grossmann, S. and Lohse, D., Torque scaling in turbulent taylor-couette flow between independently rotating cylinders, *J. Fluid Mech.*, **581**, 2007, 221–250.

[10] Flack, K. A. and Schultz, M. P., Roughness effects on wall-bounded turbulent flows, *Phys. Fluids*, **26**, 2014, 101305.

[11] Grossmann, S. and Lohse, D., Scaling in thermal convection: A unifying view, *J. Fluid. Mech.*, **407**, 2000, 27–56.

[12] Grossmann, S. and Lohse, D., Thermal convection for large Prandtl number, *Phys. Rev. Lett.*, **86**, 2001, 3316–3319.

[13] Grossmann, S. and Lohse, D., Multiple scaling in the ultimate regime of thermal convection, *Phys. Fluids*, **23**, 2011, 045108.

[14] Grossmann, S. and Lohse, D., Logarithmic temperature profiles in the ultimate regime of thermal convection, *Phys. Fluids*, **24**, 2012, 125103.

[15] Grossmann, S., Lohse, D. and Sun, C., Velocity profiles in strongly turbulent Taylor-Couette flow, *Phys. Fluids*, **26**, 2014, 025114.

[16] Grossmann, S., Lohse, D. and Sun, C., High Reynolds number Taylor-Couette turbulence, *Ann. Rev. Fluid Mech*, **48**, 2016, 53–80.

[17] He, X., Funfschilling, D., Bodenschatz, E. and Ahlers, G., Heat transport by turbulent Rayleigh-Bénard convection for $Pr = 0.8$ and $4 \times 10^{11} < Ra < 2 \times 10^{14}$: ultimate-state transition for aspect ratio $\Gamma = 1.00$, *New J. Phys..*, **14**, 2012, 063030.

[18] He, X., Funfschilling, D., Nobach, H., Bodenschatz, E. and Ahlers, G., Transition to the ultimate state of turbulent Rayleigh-Bénard convection, *Phys. Rev. Lett.*, **108**, 2012, 024502.

[19] Hewitt, D. R., Neufeld, J. A. and Lister, J. R., Ultimate regime of high rayleigh number convection in a porous medium, *Phys. Rev. Lett.*, **108**, 2012, 224503.

[20] Huang, Y.-X. and Zhou, Q., Counter-gradient heat transport in two-dimensional turbulent Rayleigh–Bénard convection, *J. Fluid Mech.*, **737**.

[21] Huisman, S. G., Scharnowski, S., Cierpka, C., Kähler, C., Lohse, D. and Sun, C., Logarithmic boundary layers in strong Taylor-Couette turbulence, *Phys. Rev. Lett.*, **110**, 2013, 264501.

[22] Jiménez, J., Turbulent flows of rough walls, *Ann. Rev. Fluid Mech.*, **36**, 2004, 173–196.

[23] Johnston, H. and Doering, C. R., Comparison of turbulent thermal convection between conditions of constant temperature and constant flux, *Phys. Rev. Lett.*, **102**, 2009, 064501.

[24] Kraichnan, R. H., Turbulent thermal convection at arbitrary Prandtl number, *Phys. Fluids*, **5**, 1962, 1374–1389.

[25] Lewis, G. S. and Swinney, H. L., Velocity structure functions, scaling, and transitions in high-Reynolds-number Couette-Taylor flow, *Phys. Rev. E*, **59**, 1999, 5457–5467.

[26] Lohse, D. and Xia, K.-Q., Small-scale properties of turbulent Rayleigh-Bénard convection, *Ann. Rev. Fluid Mech.*, **42**, 2010, 335–364.

[27] Malkus, M. V. R., The heat transport and spectrum of thermal turbulence, *Proc. R. Soc. London A*, **225**, 1954, 196–212.

[28] Marusic, I., McKeon, B. J., Monkewitz, P. A., Nagib, H. M., Smits, A. J. and Sreenivasan, K. R., Wall-bounded turbulent flows at high Reynolds numbers: Recent advances and key issues, *Phys. Fluids*, **22**, 2010, 065103.

[29] Moody, L. F., Friction factors for pipe flow, *Trans. ASME*, **66**, 1944, 671–684.

[30] Niemela, J. and Sreenivasan, K. R., Does confined turbulent convection ever attain the ?asymptotic scaling? with 1/2 power?, *New J. Phys.*, **12**, 2010, 115002.

[31] Nikuradse, J., Strömungsgesetze in rauhen Rohren, *Forschungsheft Arb. Ing.-Wes.*, **361**.

[32] Ostilla-Mónico, R., van der Poel, E. P., Verzicco, R., Grossmann, S. and Lohse, D., Boundary layer dynamics at the transition between the classical and the ultimate regime of Taylor-Couette flow, *Phys. Fluids*, **26**, 2014, 015114.

[33] Ostilla-Mónico, R., van der Poel, E. P., Verzicco, R., Grossmann, S. and Lohse, D., Exploring the phase diagram of fully turbulent Taylor-Couette flow, *J. Fluid Mech.*, **761**, 2014, 1–26.

[34] Ostilla-Mónico, R., Verzicco, R., Grossmann, S. and Lohse, D., The near-wall region of highly turbulent Taylor-Couette flow, *J. Fluid Mech.*, **788**, 2016, 95–117.

[35] Perry, A. E. and Chong, M. S., On the mechanism of wall turbulence, *J. Fluid Mech.*, **119**, 1982, 106–121.

[36] Pope, S. B., *Turbulent Flow*, Cambridge University Press, Cambridge, 2000.

[37] Priestley, C. H. B., Convection from a large horizontal surface, *Aust. J. Phys.*, **7**, 1954, 176–201.

[38] Schlichting, H. and Gersten, K., *Boundary layer theory*, Springer Verlag, Berlin, 2000, 8th edition.

[39] Schmalzl, J., Breuer, M., Wessling, S. and Hansen, U., On the validity of two-dimensional numerical approaches to time-dependent thermal convection, *Europhys. Lett.*, **67**, 2004, 390–396.

[40] See Supplemental Material at [URL will be inserted by publisher] for numerical details.

[41] Shishkina, O., Stevens, R. J. A. M., Grossmann, S. and Lohse, D., Boundary layer structure in turbulent thermal convection and its consequences for the required numerical resolution, *New J. Phys.*, **12**, 2010, 075022.

[42] Smits, A. J., McKeon, B. J. and Marusic, I., High-Reynolds Number Wall Turbulence, *Ann. Rev. Fluid Mech.*, **43**, 2011, 353–375.

[43] Spiegel, E. A., Convection in stars, *Ann. Rev. Astron. Astrophys.*, **9**, 1971, 323–352.

[44] Stevens, R. J. A. M., Lohse, D. and Verzicco, R., Prandtl and Rayleigh number dependence of heat transport in high Rayleigh number thermal convection, *J. Fluid Mech.*, **688**, 2011, 31–43.

[45] Stevens, R. J. A. M., van der Poel, E. P., Grossmann, S. and Lohse, D., The unifying theory of scaling in thermal convection: the updated prefactors, *J. Fluid Mech.*, **730**, 2013, 295–308.

[46] Stevens, R. J. A. M., Verzicco, R. and Lohse, D., Radial boundary layer structure and Nusselt number in Rayleigh-Bénard convection, *J. Fluid Mech.*, **643**, 2010, 495–507.

[47] Sun, C., Cheung, Y. H. and Xia, K.-Q., Experimental studies of the viscous boundary layer properties in turbulent Rayleigh-Bénard convection, *J. Fluid Mech.*, **605**, 2008, 79 – 113.

[48] Urban, P., Hanzelka, P., Musilová, V., Králík, T., La Mantia, M., Srnka, A. and Skrbek, L., Heat transfer in cryogenic helium gas by turbulent rayleigh–bénard convection in a cylindrical cell of aspect ratio 1, *New J. Phys.*, **16**, 2014, 053042.

[49] van der Poel, E. P., Ostilla-Mónico, R., Verzicco, R., Grossmann, S. and Lohse, D., Logarithmic mean temperature profiles and their connection to plume emissions in turbulent Rayleigh-Bénard convection, *Phys. Rev. Lett.*, **115**, 2015, 154501.

[50] van der Poel, E. P., Ostilla-Mónico, R., Verzicco, R. and Lohse, D., Effect of velocity boundary conditions on the heat transfer and flow topology in two-dimensional rayleigh-bénard convection, *Phys. Rev. E*, **90**, 2014, 013017.

[51] van der Poel, E. P., Stevens, R. J. A. M. and Lohse, D., Comparison between two- and three-dimensional Rayleigh-Bénard convection, *J. Fluid Mech.*, **736**, 2013, 177.

[52] van Gils, D. P. M., Huisman, S. G., Bruggert, G. W., Sun, C. and Lohse, D., Torque scaling in turbulent Taylor-Couette flow with co- and counter-rotating cylinders, *Phys. Rev. Lett.*, **106**, 2011, 024502.

[53] Zhang, Y., Huang, Y.-X., Jiang, N., Liu, Y.-L., Lu, Z.-M., Qiu, X. and Zhou, Q., Statistics of velocity and temperature fluctuations in two-dimensional Rayleigh-Bénard convection, *Phys. Rev. E*, **96**, 2017, 023105.

[54] Zhou, Q., Stevens, R. J. A. M., Sugiyama, K., Grossmann, S., Lohse, D. and Xia, K.-Q., Prandtl-Blasius temperature and velocity boundary layer profiles in turbulent Rayleigh-Bénard convection, *J. Fluid Mech.*, **664**, 2010, 297.

[55] Zhou, Q. and Xia, K.-Q., Measured instantaneous viscous boundary layer in turbulent Rayleigh-Bénard convection, *Phys. Rev. Lett.*, **104**, 2010, 104301.

[56] Zhu, X., Mathai, V., Stevens, R. J. A. M., Verzicco, R. and Lohse, D., Transition to the ultimate regime in two-dimensional Rayleigh-Beénard convection, *Phys. Rev. Lett.*, **120**, 2018, 144503.

[57] Zhu, X., Verschoof, R. A., Bakhuis, D., Huisman, S. G., Verzicco, R., Sun, C. and Lohse, D., Wall-roughness induces asymptotic ultimate turbulence, *Nature Physics*, **14**, 2018, 417–423.

[58] Zhu, X., Verzicco, R. and Lohse, D., Disentangling the origins of torque enhancement through wall roughness in Taylor-Couette turbulence, *J. Fluid Mech.*, **812**, 2017, 279–293.